View metadata, citation and similar papers at core.ac.uk

brought to you by CORE

provided by Elsevier - Publisher Connector

Available online at www.sciencedirect.com

SciVerse ScienceDirect

Physics Procedia 37 (2012) 851 – 858

Physics Procedia

TIPP 2011 - Technology and Instrumentation for Particle Physics 2011

Performance of LHCb Silicon Tracker detector in the LHC

Johan Luisier
On behalf of the LHCb Silicon Tracker group [1]

École Polytechnique Fédérale de Lausanne, Lausanne, Switzerland

Abstract

The LHCb experiment is designed to perform high-precision measurements of $\mathcal{CP}$ violation and search for New Physics using the enormous flux of beauty and charmed hadrons produced at the LHC. The LHCb detector is a single-arm spectrometer with excellent tracking and particle identification capabilities. The Silicon Tracker is part of the tracking system and measures very precisely the particle trajectories coming from the interaction point in the region of high occupancies around the beam axis. The LHCb Silicon Tracker covers a total sensitive area of about 12 m^2 using silicon micro-strip technology. This paper reports on the operation and performance of the Silicon Tracker during the Physics data taking at the LHC.

© 2012 Published by Elsevier B.V. Selection and/or peer review under responsibility of the organizing committee for TIPP 11. Open access under CC BY-NC-ND license.

1. Introduction

LHCb is an experiment dedicated to b physics studies at LHC [3]. Precision measurement of $\mathcal{CP}$ violation in b meson systems and searches for rare b hadron decays will be performed. The $b\bar{b}$ quark pair production at LHC peaks in the forward and backward regions (Figure 1), and therefore motivated the forward LHCb geometry. In order to reconstruct with a high precision the production and decay vertices of b-hadrons, it was decided to minimise the number of interactions in a bunch crossing to less than one, reducing the luminosity from the nominal LHC value $\mathcal{L}_{\mathrm{LHC}} = 10^{34}\ \mathrm{cm}^{-2}\,\mathrm{s}^{-1}$ to a lower one, $\mathcal{L}_{\mathrm{LHCb}} = 2{\cdot}10^{32}\ \mathrm{cm}^{-2}\,\mathrm{s}^{-1}$, by decreasing the number of interaction per bunch crossing to 0.7. However during the 2010 data taking campaign, this number was increased to 1.8. This was possible as all subdetectors were designed to cope with a peak luminosity of $\mathcal{L} = 5{\cdot}10^{32}\ \mathrm{cm}^{-2}\,\mathrm{s}^{-1}$. Despite the high occupancy, physics can still be done.

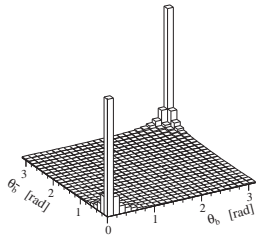

Figure 1: $b\bar{b}$ pair quark production at LHC [2].

2. The LHCb detector

The LHCb detector is a single-arm forward spectrometer. The layout is illustrated on Figure 2. The vertexing and tracking close to the interaction point is performed by a silicon micro-strip detector called the Vertex Locator (VELO). The VELO sensors are located only 8 mm away from the beam, allowing a high precision vertex reconstruction, leading to a resolution on b hadron propertime of around 50 fs.

1875-3892 © 2012 Published by Elsevier B.V. Selection and/or peer review under responsibility of the organizing committee for TIPP 11. Open access under CC BY-NC-ND license. doi:10.1016/j.phpro.2012.04.097

The charged particles are bent by a warm dipole magnet which has a field with a maximum intensity of 1.1 T. The track reconstruction uses hits in the VeLo, the Tracker Turicensis (TT), which is located upstream of the magnet and covers the full detector acceptance, and three tracking stations, downstream of the magnet. The TT is a silicon microstrip detector, described more fully in Section 3.1. The three tracking stations use two different technologies: the outer part, covering the majority of the acceptance, uses straw tubes, which offer a good spatial resolution for a reasonable cost. This detector is known as the Outer Tracker (OT). The innermost part, close to the beam pipe, has an occupancy which is much too high for drift chambers. For this reason it is covered by a silicon micro-strip detector, called Inner Tracker (IT). The Silicon Tracker (ST) consists of the IT and TT put together, and will be discussed in Section 3.

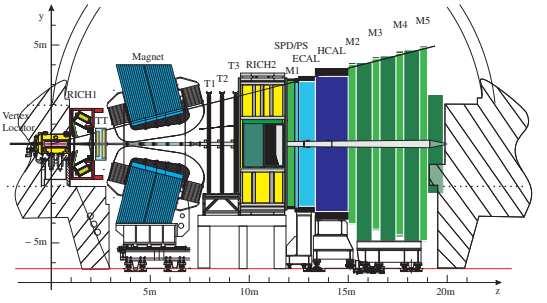

Figure 2: View of the LHCb detector in the $y - z$ plane [4].

Two RICH detectors provide particle identification. The first is located in between the VeLo and the TT, the second one after the tracking stations. They provide K/π separation in a momentum range of $1 - 150$ GeV.

The calorimeter system is situated downstream of the second RICH detector. It consists of (in order of appearance along the particles' trajectory) a scintillating pad detector (SPD), a preshower detector (PS), an electromagnetic calorimeter (ECAL), and a hadronic calorimeter (HCAL). The SPD allows to discriminate between charged and neutral electromagnetic particles, and the PS detects the showers developed in a lead converter, allowing $e^{\pm}/\pi^{\pm}$ discrimination, using again scintillators. The ECAL is made of lead and scintillator, and is optimised to reconstruct π^0. The HCAL is a sampler consisting of steel and scintillator and provides hadron identification.

Finally the muon chambers measure the muons' trajectory and provide muon identification. They are located downstream of the calorimeter system, since muons are likely to travel through the whole material of the experiment. Multiwire proportional chambers are used.

3. The Silicon Tracker

IT and TT use the same technology: both are silicon micro-strip detectors, using p-on-n sensors from Hamamatsu[1]. The electronic chain (meaning ASIC, GOL[2], DAQ boards, etc.) is the same (see Figure 3). The analog signal sent by the ASIC is carried by copper cables to the digitiser boards (located in the experimental cavern). The digital signal is then sent through optical fibres to the counting house, separated from the experiment by a concrete shielding wall, where it is processed by the TELL1 [7, 8] DAQ board.

The TT consists of one station made of four planes along the beam axis: the first and the last layers are vertical, whilst the two middle ones

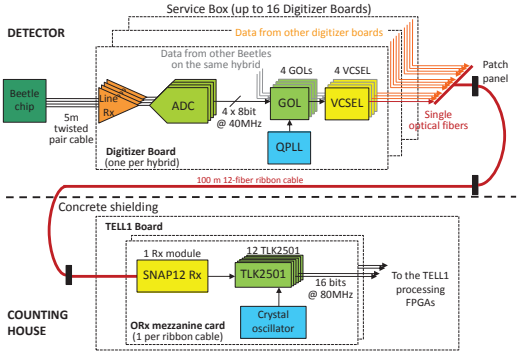

Figure 3: The Silicon Tracker readout chain [5].

[1] http://www.hamamatsu.com/
[2] Gigabit Optical Link [6].

have a stereo angle of ±5° (Figure 4a). The IT
has three stations along the beam axis, each of them consisting of four boxes, containing four layers (two vertical and two stereo ones) each. Both detectors are operated at 0°C to avoid thermal runaway.

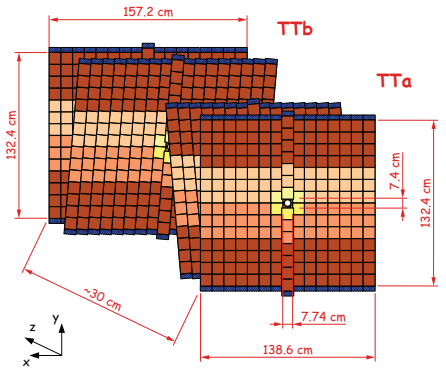

(a) Layout of the TT, the four layers are shown.

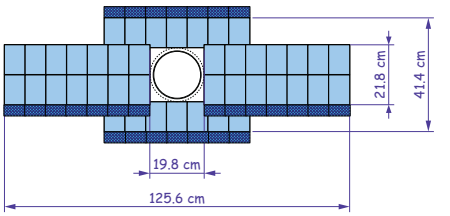

(b) Layout of the first IT station. Only the first layer is shown. In light blue are the sensors.

Figure 4: The Silicon Tracker layouts [5], in dark blue is the front-end electronics.

3.1. The Tracker Turicensis

In the TT four types of readout sectors are found: depending on the occupancy, the readout sectors consist of one, two, three or four sensors. This means the detector strips are very long, and the longest ones are 37 cm. To compensate for the noise in the four-sensor readout sectors, the thickness is 500 μm, ensuring a signal to noise ratio above 12 for any readout sector. The pitch is 183 μm, resulting of a trade-off between resolution and occupancy. The four planes represent about 8 m^2 of silicon.

The readout chips are located outside the acceptance, and are connected to the readout sectors by kapton cables.

3.2. The Inner Tracker

Each of the three IT stations consists of four boxes forming a cross-shape around the beam pipe (see Figure 4b). The boxes located above and under the beam pipe are called respectively Top and Bottom boxes and have readout sectors consisting of one 320 μm thick sensor. The readout sectors in the side boxes have two 410 μm thick sensors. The reason why those two different thicknesses is again the desired signal to noise ratio. The pitch was chosen to be 198 μm. What make this detector special in contrast to TT is the fact that the readout chips are in the boxes, i.e. in the acceptance. The twelve boxes represent an active area of about 4.3 m^2, which is about 1.3 % of the geometrical acceptance, but where 20 % of the tracks pass.

4. Performances

4.1. Current status

In the TT 99.8 % of the 143,360 strips are read out, and for IT the proportion is 98.6 % (for 129,024 strips). The missing fractions are non-working strips.

The thresholds were chosen such that the noise rate (defined as the number of noise clusters per event and per strip) is below 10^{-5}.

4.2. Time alignment

The charge collection of particles coming from a collision has to be optimised for each readout partition, because the stations have different z position, and thus different time-of-flight, and different cable lengths. The optimisation is achieved by using the so-called *time delay scan* method. Figure 5 shows in blue the readout chip pulse-shape. The purpose of optimisation is to perform the sampling at the maximum of the blue curve. Collision events are used to time align the detector with respect to the LHC collisions. To find the optimal timing data runs with collision events were collected for different clock delay phases in steps of 6.5 ns. The process is sped up by reading out successive samples spaced by 25 ns (the green lines in Figure 5). The most probable value (MPV) of the charge collection distribution was determined by fitting a Landau convoluted with a Gaussian for each delay setting and for groups of sectors corresponding to one front-end service box, such a fit is illustrated on Figure 6a.

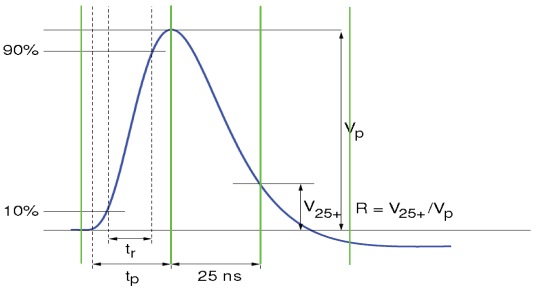

Figure 5: Readout chip pulse-shape (blue curve), overlaid with 4 sampling points (green lines).

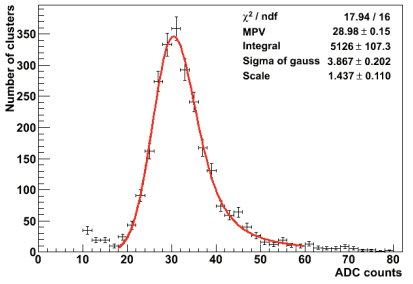

(a) Pulse height distribution for TT sensors, corresponding to one slice of the timing scan and fitted with a Landau convoluted with a Gaussian.

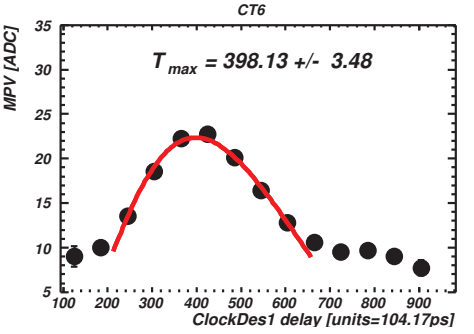

(b) MPV versus sampling time.

Figure 6: Extraction of the optimal timing.

The MPVs are then plotted versus the sampling time, and the distribution is fitted in order to extract the optimal timing (see Figure 6b). This method is applied for each readout partition, and the achieved precision is below 1 ns for both IT and TT.

4.3. Signal to noise performance

Once the detector is time aligned, the charge distribution can be looked at in order to extract the signal to noise ratio. To ensure that real signal is used in the computation, hits from tracks are used (with a momentum cut at 5 GeV). The noise is the width of the ADC distribution in absence of beam. Again a Laudau convoluted with a Gaussian is used to fit the data (Figure 7) and extract the MPV. This is done for every readout sector. In TT there are four different capacitance values for the different sector types. Since the thickness is the same, a linear dependency is expected between the signal to noise ratio and the capacitance. However the capacitance of the kapton cable connecting the sensor to the readout electronic has to be taken into account as well.

The result is presented on Figure 8a. The inversion between the three-sensor and four-sensor sector is due to the different length of the kapton cable. The three-sensor sectors have the lowest signal to noise ratio (~ 12), which fulfils the requirements.

In the IT the signal to noise ratio varies as a function of the sensor length and the thickness. Three populations are expected: the two-sensor sectors, which have higher noise and signal, the majority of one-sector sensors and there are six thick one-sensor sectors, which are expected to have higher signal to noise ratio. The results are 16.5 for the two-sensor sectors and 17.5 for the (thin) one-sensor sector, values which fulfil the requirements, and are shown in Figure 8b.

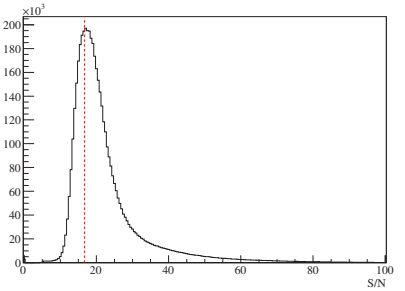

Figure 7: Fitted signal to noise ratio for an IT sector. The black line is the histogram, the red dashed line indicates the position of the fitted MPV.

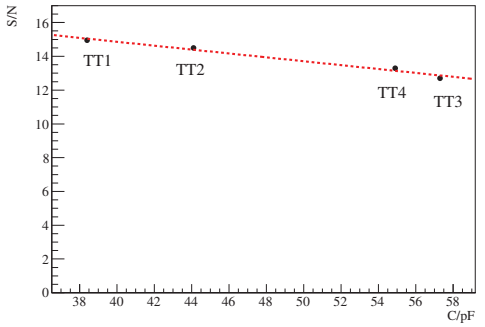

(a) Signal to noise ratio of TT readout sectors, as a function of the capacitance of the sensor.

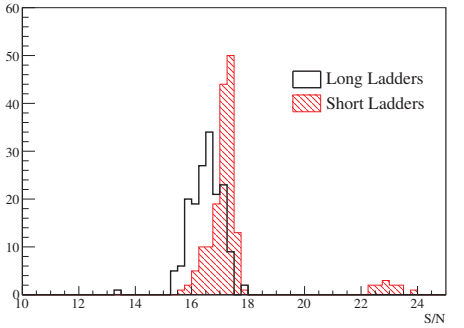

(b) Signal to noise ratio of IT readout sectors. The thick one-sensor sectors can clearly be seen on the right-hand side of the plot.

Figure 8: Signal to noise ratio for the two detectors.

4.4. Spatial alignment

The detectors have to be spatially aligned, so that the momentum measurement can be as precise as expected. The alignment is performed using a global χ^2 minimisation based on Kalman filter track fit residual [9]. For each detector element up to six degrees of freedom can be aligned (three translations and three rotations), but for some of them the sensitivity is too low, and they are therefore untouched. When the alignment is done, the *unbiased residuals* are computed for each readout sector. A residual is the distance between the fitted track and a hit belonging to the track, *unbiased* means that the track was refitted with this hit removed. The distribution of the unbiased residuals gives access to the *resolution* and the *bias*. The resolution is given by the width of the unbiased residual distribution, and carries information about the track reconstruction precision. The bias is the mean of the the unbiased residual distribution, and gives information about the precision of the alignment itself. Examples of unbiased residuals distributions are shown on Figure 9a for TT and Figure 9b for IT. Since the TT is only made out of four detector planes, a stand-alone alignment cannot be done, since it is not possible to reconstruct tracks from TT hits only. That is why the TT alignment precision is expected to be poorer than for IT, for which stand-alone reconstruction can be performed. This effect can be seen in plots showing the distribution of the biases for TT (Figure 10a) and IT (Figure 10b). The values are 17.7 μm for TT and 11.1 μm for IT.

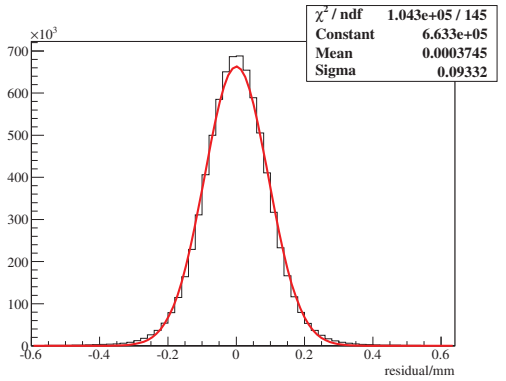

(a) Fitted TT unbiased residuals distribution for the whole detector.

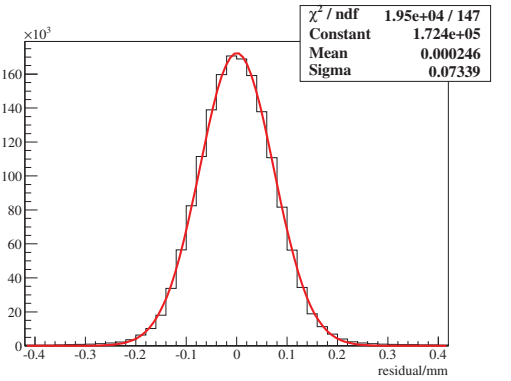

(b) Fitted IT unbiased residuals distribution for the whole detector.

Figure 9: Fitted unbiased residuals distributions, for each detectors (one entry per hit).

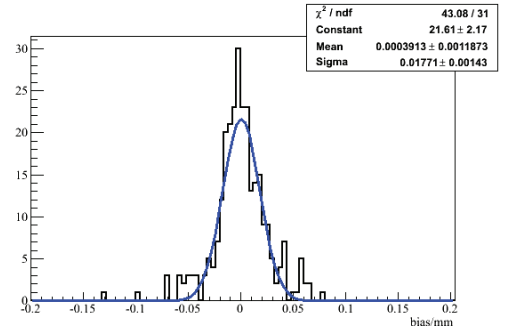

(a) TT bias per readout sector.

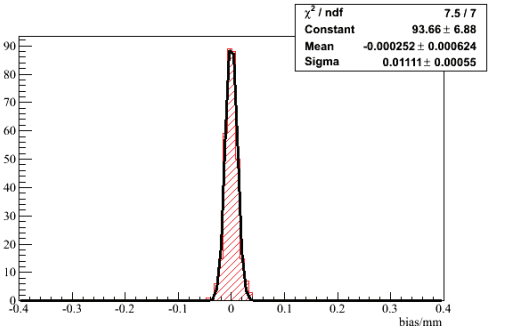

(b) IT bias per readout sector.

Figure 10: Bias per readout sector for the two detectors: this is obtained by plotting the mean of the unbiased residual distribution for each readout sector (i.e. one entry per readout sector).

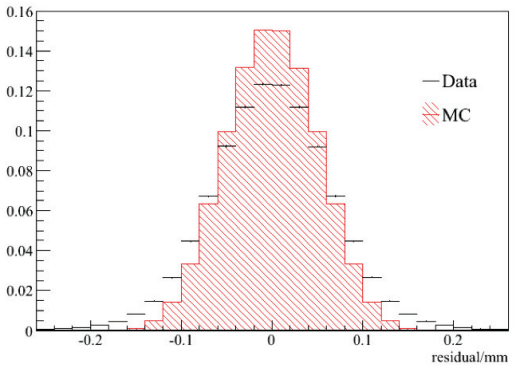

(a) TT unbiased residuals distribution.

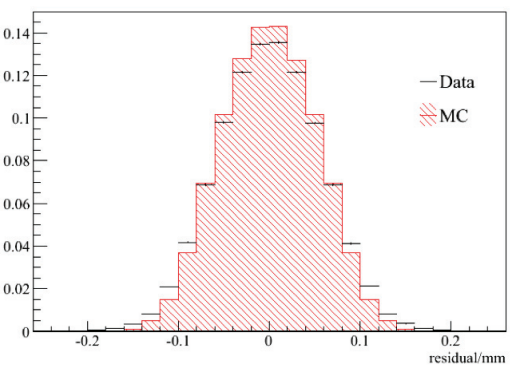

(b) IT unbiased residuals distribution.

Figure 11: Unbiased residual distributions, compared to expectations from Monte Carlo (dashed histogram).

As mentioned previously, the resolution is the width of the unbiased residuals distribution. The values are 58 μm for TT and 62 μm for IT. Figure 11a and Figure 11b show the histogram used to extract those values, compared to the unbiased residual distribution expected from Monte Carlo.

4.5. Hit efficiency

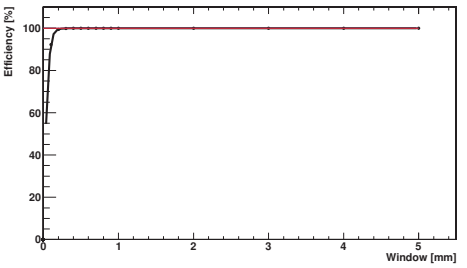

(a) Hit efficiency vs. collection window size for an IT layer.

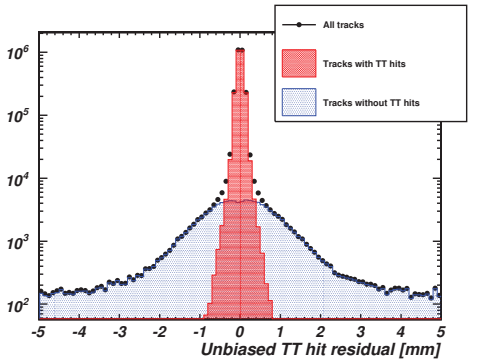

(b) TT unbiased residuals distribution for long tracks. The two Gaussian curves come from tracks without any associated TT hits and tracks with TT hits. The flat background consists of hits that do not belong to the track.

The ability of the sensors to detect a charged particle is an important quantity to measure. To do so tracks with hits in the VeLo and the tracking stations are used (called long tracks), with a tight selection on reduced track fit χ^2 and track momentum applied. In order to reject as much as possible ghost tracks, an isolation criteria is applied on top of the selection, i.e. the track will be rejected if too many hits can be found around it in a chosen window. From the detector geometry description, it is known how many hits are expected, and hits in a 'cylinder' around the track are collected. The hit efficiency is defined as the ratio between the number of found hits and the number of expected hits. Of course this efficiency varies as a function of the window size which has to be tuned. In Figure 12a, the efficiency curve saturates for a collection window size of 1 mm, and this value was chosen in the IT. This collection window is much greater than the detector resolution, because the sought hit is not necessarily associated to the track.

For TT, this is more complicated, since the used tracks may or may not have TT hits. The unbiased residuals distribution presented on Figure 12b clearly shows three populations: random hits (i.e. the flat background), tracks with TT hits (the narrow Gaussian) and tracks without TT hits (the broader Gaussian). In order to compute the hit efficiency properly, both Gaussian populations have to be taken into account, meaning that the collection window size for TT is required to be 2.5 mm. The measured efficiency is 99.3 % for TT and 99.7 % for IT.

4.6. Radiation damage

Monitoring the radiation damage is important for the ST, since the detector performance degrades with increasing radiation. Presently the radiation damage is monitored by analysing the leakage current in the different readout sectors. This study was performed with 2010 data and successfully compared to simulation done with Fluka. This agreement is qualitatively illustrated on Figure 12a and Figure 12b, which show the measured and simulated fluence respectively. Preliminary studies with this year's data for IT show that the leakage currents increase linearly with the integrated luminosity, behaviour which corresponds to expectation.

Another method is to study the *charge collection efficiency* (CCE), which consists in computing the hit finding efficiency as a function of sampling time and bias voltage. This is performed by changing the sampling time and the bias voltage only for part of the detector, and reconstruct tracks using the whole detector. Such CCE scans were performed, but the results have not been analysed yet.

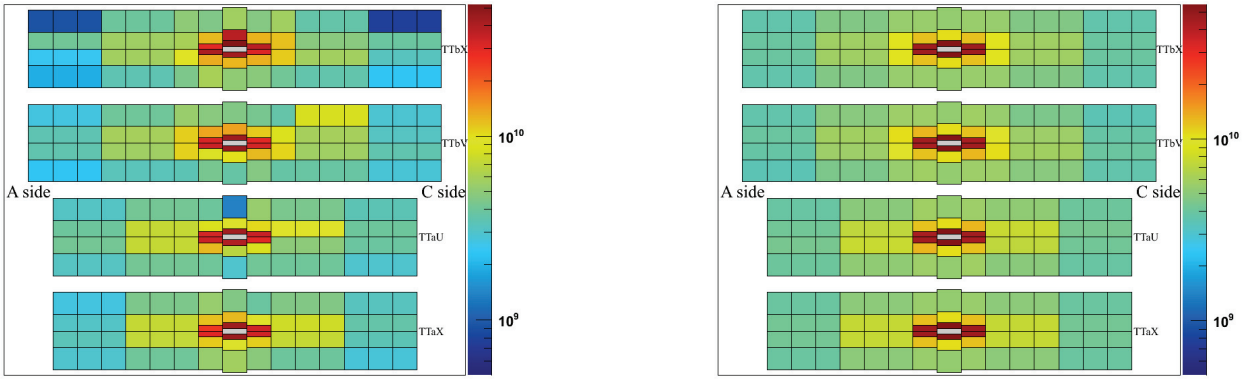

(a) Measured fluence.

(b) Simulated fluence.

Figure 12: Fluence in 1 MeV neutron equivalent in TT, log scale.

5. Conclusion

Despite the running conditions being beyond the expected values (higher interaction multiplicity, higher occupancy, ...), the LHCb Silicon Tracker is performing well and according to expectation.

The time alignment was done with high momentum tracks, achieving a precision better than 1 ns.

The signal to noise ratio was measured using high momentum tracks. The values are between 12 and 15 for TT (depending on the capacitance of the readout sector) and 16.5 for IT two-sensor sectors and 17.5 for one-sensor sectors.

The spatial alignment achieved a precision of 17.7 μm for TT and 11.17 μm for IT, the latter being more precise because it was previously internally aligned. Alignment was done using high momentum tracks and tracks from reconstructed resonances, allowing to use a mass constraint. The resolutions are in agreement with predictions from Monte Carlo simulation: 62 μm for TT and 58 μm for IT.

The sensors' ability to detect charged particles (i.e. the hit efficiency) was measured to be 99.3 % for TT and 99.7 % for IT.

Radiation damages are monitored and the measured values are in agreement with predictions.

References

[1] Tobin, M, Performance of the LHCb Silicon Tracker in pp Collisions at the LHC.
[2] LHCb : Technical Proposal, Tech. Proposal, CERN, Geneva, 1998.
[3] The LHCb collaboration et al, The LHCb Detector at the LHC, Journal of Instrumentation 3 (08) (2008) S08005. URL {http://stacks.iop.org/1748-0221/3/i=08/a=S08005}
[4] Antunes-Nobrega, R et al, LHCb reoptimized detector design and performance: Technical Design Report, Technical Design Report LHCb, CERN, Geneva, 2003.
[5] O. Steinkamp, Lhcb silicon tracker home page (Dec. 2009). URL http://lhcb.physik.uzh.ch/SiliconTracker/
[6] Cervelli, G. and Marchioro, A. and Moreira, P., A 0.13-mu-m CMOS serializer for data and trigger optical links in particle physics experiments, IEEE Trans.Nucl.Sci. 51 (2004) 836–841. doi:10.1109/TNS.2004.829551.
[7] Haefeli, G, Contribution to the development of the acquisition electronics for the LHCb experiment, Ph.D. thesis, EPFL Lausanne, Geneva (2004).
[8] Legger, F and Bay, A and Haefeli, G and Locatelli, L, TELL1 : development of a common readout board for LHCb, Tech. Rep. LHCb-2004-100. CERN-LHCb-2004-100. 1-2, CERN, Geneva (Nov 2004).
[9] W. D. Hulsbergen, The global covariance matrix of tracks fitted with a Kalman filter and an application in detector alignment, Nuclear Instruments and Methods in Physics Research A 600 (2009) 471–477. arXiv:0810.2241, doi:10.1016/j.nima.2008.11.094.